Journal of Fundamental and Applied Research **Vol. 5**, Issue 4 (2025) **20250028**

Received: 09 October 2025 / Accepted: 22 December 2025
Published online: 22 December 2025

Magnetic fields and charged particles around non-commutative black holes surrounded by an electric current loop

Ozodbek Abdurakhmonov[1, 2, *]

[1] *Institute of Fundamental and Applied Research, National Research University TIIAME, Kori Niyoziy 39, Tashkent 100000, Uzbekistan*
[2] *Institute of Nuclear Physics, Ulugbek 1, Tashkent 100214, Uzbekistan*

Abstract Noncommutative (NC) geometry provides an elegant framework for addressing quantum-gravitational corrections at the Planck scale, thereby introducing a fundamental length scale that regularizes spacetime singularities in black-hole solutions. In this work, we investigate the electromagnetic and dynamical properties of charged test particles around non-commutative black holes surrounded by an electric current loop positioned at the innermost stable circular orbit (ISCO). We derive exact analytical solutions to the Maxwell equations for the electromagnetic four-potential and magnetic-field components in both the interior and exterior regions of the current loop, thereby extending Petterson's pioneering approach to the NC geometry framework. The resulting magnetic field configuration exhibits a quasi-uniform structure inside the loop and dipolar behavior in the exterior region, with both components being significantly modified by the non-commutative parameter Θ. We analyze the effective potential governing charged-particle motion and determine the characteristic orbital parameters, including the ISCO radius, angular momentum, energy, and energy efficiency, as functions of both the radial coordinate and the NC parameter. Our results demonstrate that increasing Θ systematically modifies the spacetime structure, leading to measurable deviations in particle dynamics and magnetic field configurations. These findings provide testable signatures of noncommutative geometry effects in the strong-field regime around astrophysical black holes and contribute to understanding the interplay between quantum-gravity corrections and electromagnetic phenomena in extreme gravitational environments.

Key words: Black hole, ISCO, Noncommutative geometry, Maxwell equations, charged particle dynamics.

I. INTRODUCTION

The study of black holes in extreme gravitational environments represents one of the most fascinating frontiers in contemporary theoretical physics. While General Relativity (GR) has achieved remarkable success in describing gravitational phenomena at astrophysical scales, it predicts the existence of spacetime singularities at the centers of black holes where classical physics breaks down [1]. The resolution of these singularities requires a quantum theory of gravity, yet a complete and consistent framework remains elusive. In this context, noncommutative (NC) geometry has emerged as a promising approach for incorporating quantum-gravitational effects at the Planck scale [2, 3].

The pioneering work of Nicolini and collaborators [2, 4, 5] demonstrated that non-commutative geometry provides an elegant mechanism for regularizing black hole singularities by introducing a fundamental length scale into the spacetime structure. This approach, inspired by string theory and M-theory considerations [6, 7], replaces the point-like mass distribution with a Gaussian-smeared mass density characterized by a non-commutative parameter Θ. The resulting black hole solutions exhibit remarkable properties: they are singularity-free, possess a de Sitter core at small scales, and smoothly transition to the classical Schwarzschild or Reissner-Nordström geometries at large distances [8, 9]. Recent observational constraints and theoretical investigations have renewed interest in NC black holes as viable alternatives to classical solutions, with potential observational signatures in strong-field regimes [10, 11].

Alongside the geometric properties of spacetime, electromagnetic phenomena play a crucial role in understanding black hole physics and their astrophysical manifestations. The interaction between black holes and magnetic fields is fundamental to explaining energy extraction mechanisms, jet formation, and particle acceleration processes observed in active galactic nuclei

* Corresponding author: ozodbek992606@gmail.com

and X-ray binaries [12, 13]. The seminal work of Wald [13] established the exact solution for the electromagnetic field of a rotating black hole immersed in an asymptotically uniform magnetic field, revealing the existence of a gravitationally induced electric field with profound implications for black hole electrodynamics. Petterson [14] extended this analysis by deriving the magnetic field configuration generated by a current loop positioned in the equatorial plane of a Schwarzschild black hole, demonstrating that the field exhibits quasi-uniform behavior inside the loop and dipolar structure in the exterior region.

The study of charged-particle dynamics around magnetized black holes has attracted considerable attention due to its relevance to accretion disk physics and high-energy phenomena. Extensive investigations have been conducted on particle motion in various black hole spacetimes immersed in external magnetic fields [15–17]. Recent work has explored the effects of modified gravity theories and quantum corrections on charged particle trajectories and the innermost stable circular orbit (ISCO) radius [18–20]. The ISCO plays a critical role in accretion disk theory, as it defines the inner boundary of the disk and determines the efficiency of energy extraction through the Novikov-Thorne mechanism [21, 22]. Understanding how quantum-gravitational corrections modify the ISCO and related orbital parameters is essential for interpreting observational data from black hole systems and for potentially distinguishing among different gravity theories.

Despite extensive research on NC black holes and on electromagnetic phenomena around classical black holes, a comprehensive investigation of electromagnetic fields and charged-particle dynamics in NC black-hole spacetimes with realistic magnetic-field configurations remains lacking. Previous studies have primarily focused on either the geometric properties of NC black holes [23, 24] or particle dynamics in classical black hole magnetospheres [25, 26]. The present work addresses this gap by extending Petterson's pioneering approach [14] to the framework of noncommutative geometry, thereby deriving exact analytical solutions to Maxwell's equations for a current loop located at the ISCO of an NC black hole.

In this paper, we investigate the electromagnetic and dynamical properties of charged test particles around non-commutative black holes surrounded by an electric current loop positioned at the innermost stable circular orbit. Our analysis encompasses several key aspects: (i) derivation of exact solutions to Maxwell's equations for the electromagnetic four-potential and magnetic field components in both the interior and exterior regions of the current loop; (ii) comprehensive analysis of the magnetic field structure and its modification due to the non-commutative parameter Θ; (iii) investigation of the effective potential governing charged particle motion and determination of characteristic orbital parameters including ISCO radius, angular momentum, and energy; and (iv) evaluation of energy efficiency in the context of accretion disk physics. Our results demonstrate that the noncommutative parameter systematically modifies the spacetime structure, leading to measurable deviations in both magnetic field configurations and particle dynamics, thereby providing testable signatures of quantum-gravitational effects in the strong-field regime around astrophysical black holes.

II. BLACK HOLES IN NC GRAVITY

The spacetime of the spherically symmetric spacetime around black holes in Non-Commutative geometry is described through the spherical coordinates $x^\alpha = \{t, r, \theta, \phi\}$ by the line element [2]:

$$ds^2 = -f(r)dt^2 + \frac{1}{f(r)}dr^2 + r^2\left(d\theta^2 + \sin^2\theta d\phi^2\right), \tag{1}$$

where the lapse function is

$$f(r) = 1 - \frac{2M}{r} + \frac{8M\sqrt{\Theta}}{\sqrt{\pi}r^2}, \tag{2}$$

where Θ is the Non-Commutative parameter, $[\Theta] = M^2$.

The standard mathematical way of determining the event horizon is $g_{rr} \to \infty$ ($g^{rr} = 0$) or equivalently $f(r) = 0$ and we have the radius of event horizon at

$$r_\pm = M \pm \frac{\sqrt{M}\sqrt{\sqrt{\pi}M - 8\sqrt{\Theta}}}{\sqrt[4]{\pi}} \tag{3}$$

so, in GR ($\Theta \to 0$) it takes $r_h = 2M$.

III. MAGNETIC FIELD SOLUTIONS OF MAXWELL EQUATIONS IN SPACETIME AROUND BLACK HOLES IN NC GRAVITY

In this section, we seek solutions to Maxwell's equations that describe the magnetic field generated by a current loop in the vicinity of static black holes within aether theory. Petterson initially examined the problem in the context of Schwarzschild spacetime in Ref. [14]. When expressed in curved spacetime, Maxwell's equations assume the following form:

$$\partial_\mu(\sqrt{-g}F^{\mu\nu}) = 4\pi\sqrt{-g}J^\nu, \quad \partial_\mu(\sqrt{-g}\,{}_*F^{\mu\nu}) = 0 \tag{4}$$

In these equations, $F^{\mu\nu}$ represents the electromagnetic field tensor, with its dual given by ${}_*F^{\mu\nu} = \frac{1}{2!}\epsilon^{\mu\nu\gamma\rho}F_{\gamma\rho}$. The tensor $\eta_{\alpha\beta\sigma\gamma}$ can be written in terms of the Levi-Civita antisymmetric symbol $\epsilon_{\alpha\beta\sigma\gamma}$ as:

$$\eta_{\alpha\beta\sigma\gamma} = \sqrt{-g}\epsilon_{\alpha\beta\sigma\gamma}\,, \qquad \eta^{\alpha\beta\sigma\gamma} = -\frac{1}{\sqrt{-g}}\epsilon^{\alpha\beta\sigma\gamma}\,, \tag{5}$$

with the metric tensor determinant from (1) being $g = -r^4\sin^2\theta$. The four-current vector J^μ serves as the source term for the black hole's magnetic field. We assume a current-carrying loop positioned in the equatorial plane near the innermost stable circular orbit ($r_0 = r_{ISCO}$), with the electric current possessing solely an azimuthal component ($J^t = J^r = J^\theta = 0$):

$$J^\phi = \frac{I}{r^2}\sqrt{f(r)}\delta(r - r_0)\delta(\cos\theta)\,. \tag{6}$$

Obtaining analytical solutions to Maxwell's equations requires exploiting the symmetry properties of the spacetime metric to enable separation of variables in the differential equations. For instance, in his groundbreaking work on black hole electrodynamics, R. Wald derived exact solutions by utilizing time-like and space-like Killing vectors associated with the spacetime's axial symmetry.

Given the loop's equatorial placement and the spacetime's axially symmetric nature, we can treat the vector potential as dependent solely on the r and θ coordinates ($A_\phi(r,\theta)$). For axially symmetric and stationary electromagnetic fields, the Maxwell equation in Eq.(4) becomes the following in the spacetime (1):

$$\begin{aligned}\frac{1}{\sin\theta}\frac{\partial}{\partial r}\Big(f(r)\frac{\partial}{\partial r}A_\phi(r,\theta)\Big) \;+\; & \frac{1}{r^2\sin\theta}\frac{\partial}{\partial\theta}\Big(\frac{1}{\sin\theta}\frac{\partial}{\partial\theta}A_\phi(r,\theta)\Big) \\ = \;& -4\pi I\sqrt{f(r)}\delta(r-r_0)\delta(\cos\theta)\,.\end{aligned} \tag{7}$$

We seek a solution to Eq.(7) that can be expressed in separable form:

$$A_\phi(r,\theta) = \mathcal{R}(r)\Theta(\theta)\,, \tag{8}$$

which yields two decoupled equations:

$$\sin\theta\frac{d}{d\theta}\Big(\frac{1}{\sin\theta}\frac{d\Theta_l(\theta)}{d\theta}\Big) + (l+1)(l+2)\Theta_l(\theta) = 0\,, \tag{9}$$

$$r^2\frac{d}{dr}\Big(f(r)\frac{d\mathcal{R}_l(r)}{dr}\Big) - (l+1)(l+2)\mathcal{R}_l(r) = 0\,, \tag{10}$$

where l denotes the multipole number, restricted to integer values. Solving Eqs. (9) and (10) for general values of l proves quite involved. Therefore, we simplify by focusing on the $l = 0$ case. Henceforth, we denote $\mathcal{R}_0(r)$ simply as $\mathcal{R}(r)$ and $\Theta_0(\theta)$ as $\Theta(\theta)$. For this case, Eq.(10) yields the regular solution $\Theta(\theta) = \sin^2\theta$, reducing the radial function equation to:

$$\Big[(r-M)^2 - M^2(1-\alpha)\Big]\mathcal{R}''(r) + 2M\left(1+\alpha\frac{M}{r}\right)\mathcal{R}'(r) - 2\mathcal{R}(r) = 0\,. \tag{11}$$

Upon solving Eq.(11), we obtain the vector potential through the following procedure:

$$\begin{aligned}A_\phi = & -\frac{3\mu\sin^2\theta}{8(1+\alpha)^{3/2}M^3}(r^2+\alpha M^2) \\ & \times\left[\frac{2\sqrt{1+\alpha}M(r_0+2M)}{r_0^2+\alpha M^2} + \ln\left(1 - \frac{2M\sqrt{1+\alpha}}{r_0 - M(1-\sqrt{1+\alpha})}\right)\right], \quad r_+ \le r \le r_0\end{aligned} \tag{12}$$

$$A_\phi = -\frac{3\mu\sin^2\theta}{8(1+\alpha)^{3/2}M^3}(r^2+\alpha M^2) \times \left[\frac{2\sqrt{1+\alpha}M(r+2M)}{r^2+\alpha M^2} + \ln\left(1-\frac{2M\sqrt{1+\alpha}}{r-M(1-\sqrt{1+\alpha})}\right)\right], \quad r \geq r_0 \tag{13}$$

where the current loop around the aether BH is responsible for the magnetic moment μ:

$$\mu = \pi r_0^2\sqrt{f(r_0)}I\left(1+\alpha\frac{M^2}{r_0^2}\right). \tag{14}$$

Now, it is possible to get non-zero components of the magnetic field around the ather BH in the interior and exterior regions of the ISCO, where the current loop is located using the expression Ref. [27] $B^\alpha = (1/2)\eta^{\alpha\beta\gamma\sigma}F_{\beta\gamma}u_\sigma$, with respect to proper observer, where $u_\sigma = -\sqrt{f(r)}(1,0,0,0)$, in the following form [28]:

$$B^{\hat{r}}_{in} = B_{in}\left(1+\alpha\frac{M^2}{r^2}\right)\cos\theta\,, \tag{15}$$

$$B^{\hat{\theta}}_{in} = B_{in}\sqrt{f(r)}\sin\theta\,, \tag{16}$$

with

$$B_{in} = -\frac{3}{4}\frac{\mu}{(1+\alpha)^{\frac{3}{2}}M^3}\left[\frac{2\sqrt{1+\alpha})M(r_0+M)}{r_0^2+\alpha M^2} + \ln\left(1-\frac{2M\sqrt{1+\alpha}}{r_0-M(1-\sqrt{1+\alpha})}\right)\right], \tag{17}$$

and

$$B^{\hat{r}}_{ex} = -\frac{3}{4}\frac{\mu\cos\theta}{(1+\alpha)^{\frac{3}{2}}M^3}\left[\frac{2\sqrt{1+\alpha})M}{r}\left(1+\frac{M}{r}\right) + \left(1+\alpha\frac{M^2}{r^2}\right)\ln\left(1-\frac{2M\sqrt{1+\alpha}}{r-M(1-\sqrt{1+\alpha})}\right)\right]$$

$$B^{\hat{\theta}}_{ex} = \frac{3}{4}\frac{\mu\sin\theta}{(1+\alpha)^{\frac{3}{2}}M^3}\left[\frac{2\sqrt{1+\alpha})M}{r\sqrt{f(r)}}\left(1-\frac{M}{r}\right) + \sqrt{f(r)}\ln\left(1-\frac{2M\sqrt{1+\alpha}}{r-M(1-\sqrt{1+\alpha})}\right)\right],$$

respectively.

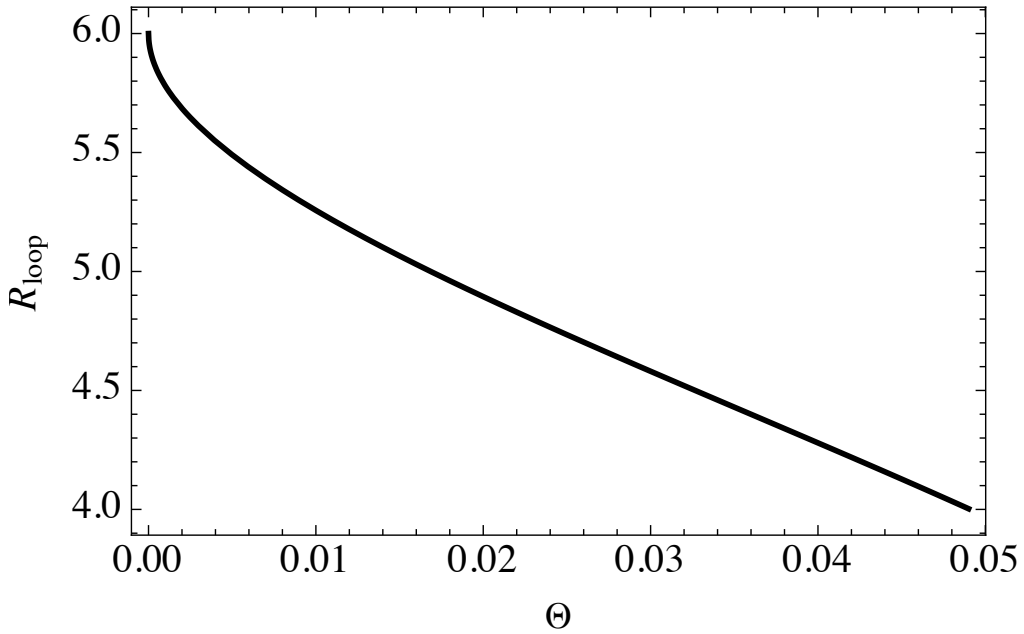

FIG. 1: Graphical illustration of the loop radius along Θ.

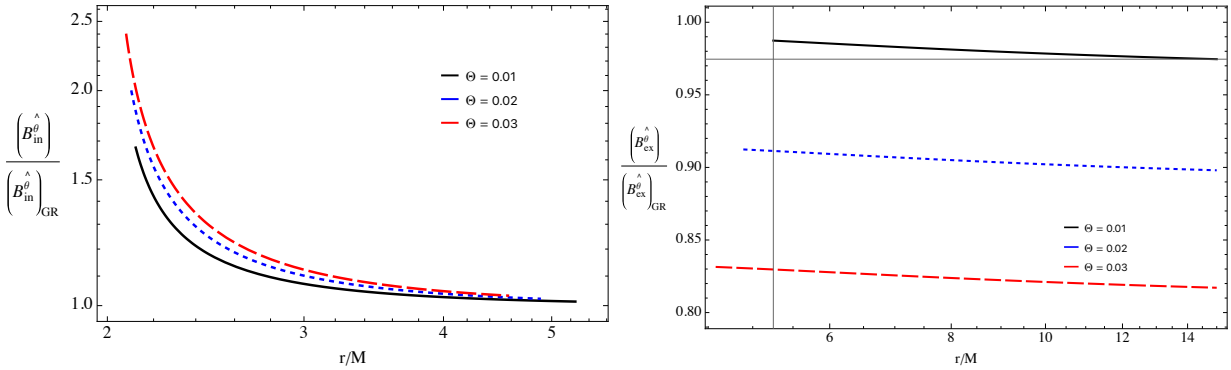

FIG. 2: Variation of the normalized magnetic field component $B^{\hat{\theta}}$ in the interior region (left) and exterior region (right) as functions of the radial coordinate r/M, for different values of the non-commutative parameter Θ.

In Fig 1 We can easily see, the loop radius shows a monotonic decrease as Θ increases.

Fig. 2 displays the angular component of the magnetic field $\hat{B}^{\hat{\theta}}$ normalized to the GR case for the interior (left panel, $r_+ \leq r \leq r_0$) and exterior (right panel, $r \geq r_0$) regions of the current loop. The profiles are shown for three values of the NC parameter: $\Theta = 0.01M^2$ (black line), $\Theta = 0.02M^2$ (blue line), and $\Theta = 0.03M^2$ (red line). In the interior region, the magnetic field strength increases monotonically with radius. It is significantly enhanced compared to GR, with larger values of Θ producing stronger deviations—reaching ratios up to 2.5 at $r \approx 5M$ for $\Theta = 0.03M^2$. Conversely, in the exterior region, the magnetic field is suppressed relative to GR, with the suppression being more pronounced for larger Θ values. The exterior field gradually converges to the GR limit at large distances ($r \gtrsim 14M$), demonstrating that NC effects are localized to the strong-field regime near the black hole.

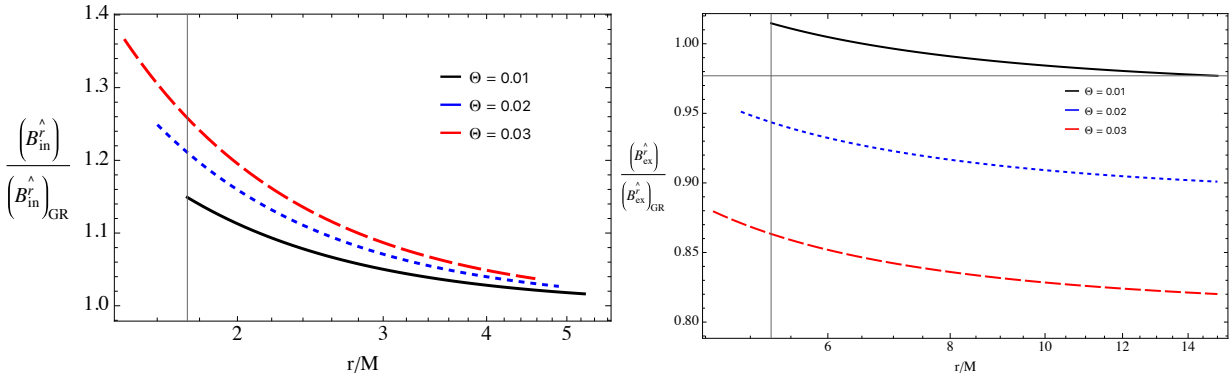

FIG. 3: Variation of the normalized magnetic field component $B^{\hat{r}}$ in the interior region (left) and exterior region (right) as functions of the radial coordinate r/M, for different values of the non-commutative parameter Θ.

Fig. 3 presents the radial component of the magnetic field $\hat{B}^{\hat{r}}$ normalized to the GR case for the interior (left panel, $r_+ \leq r \leq r_0$) and exterior (right panel, $r \geq r_0$) regions of the current loop. The profiles correspond to three values of the NC parameter: $\Theta = 0.01M^2$ (black line), $\Theta = 0.02M^2$ (blue line), and $\Theta = 0.03M^2$ (red line). In the interior region, the radial magnetic field component exhibits a modest enhancement compared to GR, with the normalized ratio $\hat{B}^{\hat{r}}_{in}/\hat{B}^{\hat{r}}_{GR}$ reaching approximately 1.4 at $r \approx 5M$ for $\Theta = 0.03M^2$. The enhancement grows monotonically with radius and becomes more pronounced for larger values of Θ. In the exterior region, as with the angular component, the radial field is suppressed relative to GR, with the suppression increasing for higher Θ. The exterior field asymptotically approaches the GR limit at large distances ($r \gtrsim 14M$), confirming that NC modifications are predominantly effective in the vicinity of the black hole.

IV. DYNAMICS OF TEST PARTICLES AROUND NC BHS

Now, we investigate the dynamics of electrically charged test particles around an aether BH, paying our attention to considering only circular stable orbits.

The Lagrangian for test particles with rest mass m, orbiting a BH reads as [29]

$$L_{\rm p} = \frac{1}{2} m g_{\mu\nu} \dot{x}^{\mu} \dot{x}^{\nu}. \tag{18}$$

It isn't easy to find analytical solutions to the equations of motion unless integrals of motion are introduced. Fortunately, in an axially symmetric and stationary spacetime, it is possible to introduce the Killing vectors generated by the symmetry of the spacetime, which are responsible for the conservation of energy and angular momentum of the particle along the geodesic motion.

The corresponding conserved quantities can be calculated using the Killing vectors,

$$\xi^{\mu}_{(t)} \partial_{\mu} = \partial_t, \qquad \xi^{\mu}_{(\phi)} \partial_{\mu} = \partial_{\phi}, \tag{19}$$

where $\xi^{\mu}_{(t)} = (1,\ 0,\ 0,\ 0)$ and $\xi^{\mu}_{(\phi)} = (0,\ 0,\ 0,\ 1)$, which are corresponding to the energy and angular momentum of the particles $\mathcal{E} = E/m$ and $\mathcal{L} = L/m$, respectively, with equations,

$$\dot{t} = \frac{\mathcal{E}}{g_{tt}}, \quad \dot{\phi} = \frac{\mathcal{L}}{g_{\phi\phi}}. \tag{20}$$

Here, we derive the equations of motion using the following normalization condition,

$$g_{\mu\nu} u^{\mu} u^{\nu} = -1. \tag{21}$$

Equations of motion for test particles that are around a static BH take the following form using Eqs. (20) and (21),

$$\dot{r}^2 \ = \ \mathcal{E}^2 + g_{tt} \left(1 + \frac{\mathcal{K}}{r^2} \right) , \tag{22}$$

$$\dot{\theta}^2 \ = \ \frac{1}{g^2_{\theta\theta}} \Big(\mathcal{K} - \frac{\mathcal{L}^2}{\sin^2 \theta} \Big) , \tag{23}$$

with the Carter constant $\mathcal{K}$.

In this work, we investigate the particle's motion in the constant plane $p_{\theta} = 0$. At the equatorial plane, the constant $\mathcal{K}$ will be $\mathcal{K} = \mathcal{L}^2$ and one can get,

$$\dot{r}^2 = \mathcal{E}^2 - V_{\rm eff} \tag{24}$$

where $V_{\rm eff}$ is the effective potential, and it has the following form,

The effective potential for the interior region ($r_+ \leq r \leq r_0$) is given by:

$$V^{\rm in}_{\rm eff}(r) = \frac{f(r)}{r^2} \left(L + \frac{R^2 \sqrt{f(R)} \left(1 + \frac{\alpha M^2}{R^2} \right) \left(r^2 + \alpha M^2 \right) \mathcal{F}(R) \omega}{(1+\alpha)^{3/2}} \right)^2 + f(r), \tag{25}$$

where

$$f(r) = 1 - \frac{2M}{r} + \frac{\alpha M^2}{r^2}, \tag{26}$$

$$\mathcal{F}(R) = \frac{2\sqrt{1+\alpha} M (R + 2M)}{R^2 + \alpha M^2} + \ln \left(1 - \frac{2M\sqrt{1+\alpha}}{R - M(1 - \sqrt{1+\alpha})} \right), \tag{27}$$

and

$$\alpha(M, \Theta) = \frac{8\sqrt{\Theta}}{M\sqrt{\pi}}. \tag{28}$$

is a new constant.

In the above expression, $\omega = eB/(2m)$ is responsible for the magnetic interaction between the particle's electric charge and external magnetic fields. In our further analysis, we assume the current loop's position at $r_0 = 6M$. The effective potential for the exterior region ($r \geq r_0$) takes the form:

$$V_{\text{eff}}^{\text{ex}}(r) = \frac{f(r)}{r^2}\left(L + \frac{\omega R^2\sqrt{f(R)}\left(1+\frac{\alpha M^2}{R^2}\right)\left(r^2+\alpha M^2\right)\mathcal{R}(r)}{(1+\alpha)^{3/2}}\right)^2 + f(r), \tag{29}$$

where

$$\mathcal{R}(r) = \frac{2\sqrt{1+\alpha}M(r+2M)}{r^2+\alpha M^2} + \ln\left(1 - \frac{2M\sqrt{1+\alpha}}{r - M(1-\sqrt{1+\alpha})}\right), \tag{30}$$

with $f(r)$ and α defined as above. Here, $R = r_0$ denotes the radius of the current loop at ISCO, L is the angular momentum, and ω is the angular frequency parameter.

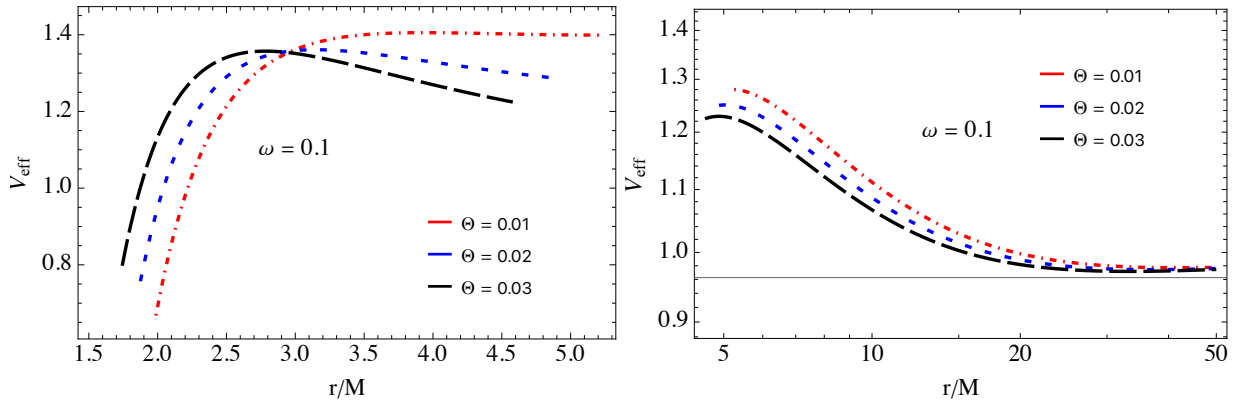

FIG. 4: Variation of effective potential the interior region (left) and exterior region (right) as functions of the radial coordinate r/M, for different values of the non-commutative parameter Θ.

A. Effective potential

Fig. 4 illustrates the effective potential V_{eff} for test particle motion in the interior (left panel, $1.5M \lesssim r \lesssim 5M$, with $\omega = 0.1$) and exterior (right panel, $r \gtrsim 5M$) regions around NC black holes. The profiles are displayed for three values of the NC parameter: $\Theta = 0.01M^2$ (red line), $\Theta = 0.02M^2$ (blue line), and $\Theta = 0.03M^2$ (black line). In the interior region, the effective potential exhibits a characteristic barrier structure with a maximum around $r \approx 3M$. As Θ increases, the potential barrier becomes more pronounced, with V_{eff} reaching higher values for larger NC parameters—the black curve ($\Theta = 0.03M^2$) attains approximately $V_{\text{eff}} \approx 1.4$ at the peak. In contrast, the red curve ($\Theta = 0.01M^2$) reaches only $V_{\text{eff}} \approx 1.2$. This enhancement indicates that NC effects strengthen the effective gravitational barrier, potentially affecting the stability and location of circular orbits near the black hole. In the exterior region, the effective potential decreases monotonically with radius and shows a clear separation between different Θ values at intermediate distances. Higher values of Θ correspond to elevated potential values, with the black curve ($\Theta = 0.03M^2$) maintaining the highest potential throughout the plotted range. All curves exhibit logarithmic decay behavior at large radial distances, asymptotically approaching unity as $r \to \infty$, which reflects the diminishing influence of NC corrections in the weak-field regime.

B. Angular momentum

To study the circular motion of the test particle, consequently, we consider the conditions that imply there are no radial motion ($\dot{r} = 0$) and no forces in the radial direction ($\ddot{r} = 0$) [30]. Using this condition, one can get expressions for the specific angular

momentum and a specific energy for circular orbits in the equatorial plane ($\theta = \pi/2$) where the effective potential as given in Eq.(25) and (29) is maximal

$$\mathcal{L}^2(r) = \frac{Mr^2(\alpha M + r)}{-2\alpha M^2 - 3Mr + r^2}\,, \qquad \mathcal{E}^2(r) = \frac{\left(\alpha M^2 + 2Mr - r^2\right)^2}{r^2\left(-2\alpha M^2 - 3Mr + r^2\right)}\,, \tag{31}$$

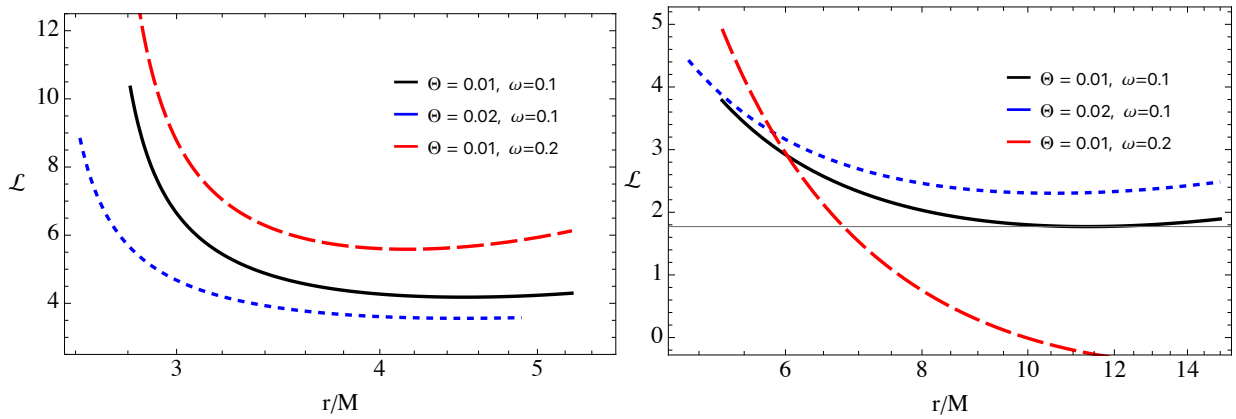

FIG. 5: Variation of angular momentum the interior region (left) and exterior region (right) as functions of the radial coordinate r/M, for different values of the non-commutative parameter Θ and ω.

Fig. 5 presents the specific angular momentum $\mathcal{L}$ of charged test particles as a function of radial coordinate for the interior (left panel, $3M \lesssim r \lesssim 5M$) and exterior (right panel, $r \gtrsim 6M$) regions around NC black holes. The profiles are shown for three parameter combinations: $\Theta = 0.01M^2$, $\omega = 0.1$ (black line), $\Theta = 0.02M^2$, $\omega = 0.1$ (blue line), and $\Theta = 0.01M^2$, $\omega = 0.2$ (red line). In the interior region, the angular momentum increases monotonically with radius for all configurations, reflecting the requirement for higher angular momentum to maintain stable circular orbits at larger radii in the strong-field regime. The red curve exhibits significantly higher angular momentum values, reaching $\mathcal{L} \approx 12M$ at $r \approx 5M$, compared to the black curve which attains $\mathcal{L} \approx 4M$ at the same location. This substantial enhancement demonstrates that particle charge dramatically increases the angular-momentum requirements for circular orbits due to electromagnetic interaction with the magnetic field. The blue curve lies between the black and red curves, indicating that increasing the NC parameter also increases the required angular momentum, albeit to a lesser extent than doubling the particle charge. In the exterior region, the angular momentum exhibits distinct behavior across different radial ranges. At intermediate distances ($6M \lesssim r \lesssim 10M$), all three curves show rapid growth, with the red curve maintaining the highest values throughout. Beyond $r \approx 10M$, the angular momentum profiles begin to level off and eventually decrease, asymptotically approaching zero at large distances. This behavior reflects the transition from the strong-field regime, in which electromagnetic and NC effects are significant, to the weak-field regime, in which Newtonian dynamics dominate. The ordering of the curves (red $>$ blue $>$ black) is preserved throughout the exterior region, confirming that both particle charge and the NC parameter play persistent roles in determining the orbital characteristics of charged particles around NC black holes.

V. CONCLUSION

In this work, we have conducted a comprehensive investigation of electromagnetic field configurations and charged-particle dynamics around noncommutative black holes with a current loop at the innermost stable circular orbit. By extending Petterson's classical approach to the framework of non-commutative geometry, we have derived exact analytical solutions to Maxwell's equations that describe the magnetic field both interior and exterior to the current loop in NC black hole spacetime, characterized by the metric proposed by Nicolini and collaborators.

Our analysis reveals several significant findings regarding the influence of the non-commutative parameter Θ on electromagnetic phenomena and particle dynamics in the strong gravitational field regime:

Magnetic Field Structure: The magnetic field configuration exhibits qualitatively distinct behavior in the interior and exterior regions of the current loop, with both components being substantially modified by quantum gravitational corrections encoded in the parameter Θ. In the interior region ($r_+ \leq r \leq r_0$), the magnetic field components show monotonic enhancement compared to the classical General Relativity case, with the angular component $B^{\hat{\theta}}$ reaching normalized ratios up to 2.5 for $\Theta = 0.03M^2$ at $r \approx 5M$ (Figure 2). Similarly, the radial component $B^{\hat{r}}$ exhibits modest but systematic enhancement, with normalized

ratios approaching 1.4 under comparable conditions (Figure 3). Conversely, in the exterior region ($r \geq r_0$), both magnetic field components are suppressed relative to the GR predictions, with the suppression being more pronounced for larger values of Θ. The asymptotic convergence to GR values at large distances ($r \gtrsim 14M$) confirms that NC effects are predominantly confined to the strong-field regime near the black hole horizon, consistent with the expected behavior of quantum gravitational corrections.

Current Loop Radius: The position of the ISCO, and consequently the current loop radius, decreases monotonically with increasing Θ (Figure 1), indicating that quantum gravitational corrections enhance the gravitational binding and allow stable circular orbits to exist at smaller radii. This behavior is fundamentally different from modifications induced by black hole spin or charge, providing a potential discriminant for NC effects in observational contexts.

Effective Potential and Orbital Stability: The effective potential governing charged particle motion exhibits significant modifications due to both the non-commutative parameter and electromagnetic interactions (Figure 4). In the interior region, the potential barrier becomes more pronounced with increasing Θ, with the maximum value of V_{eff} rising from approximately 1.2 for $\Theta = 0.01M^2$ to 1.4 for $\Theta = 0.03M^2$ at the characteristic radius $r \approx 3M$. This enhancement of the potential barrier has essential implications for the stability and location of circular orbits near the black hole. In the exterior region, the effective potential shows a clear separation among different Θ values at intermediate distances, with higher NC parameters corresponding to higher potential values. The monotonic decrease and asymptotic approach to unity at large radial distances reflect the diminishing influence of quantum corrections in the weak-field regime.

Angular Momentum Requirements: The specific angular momentum required to maintain circular orbits shows strong dependence on both the non-commutative parameter and the electromagnetic coupling parameter ω (Figure 5). In the interior region ($3M \lesssim r \lesssim 5M$), particles with higher charge-to-mass ratios (larger ω) require substantially greater angular momentum, with values reaching $\mathcal{L} \approx 12M$ for $\omega = 0.2$ compared to $\mathcal{L} \approx 4M$ for $\omega = 0.1$ at $r \approx 5M$. The increase of the NC parameter also elevates the required angular momentum, though to a lesser extent than electromagnetic effects. In the exterior region, the angular-momentum profiles exhibit rapid growth at intermediate distances, followed by an asymptotic decrease at large radii, confirming the transition from strong-field to weak-field regimes. The consistent ordering of curves (with higher ω and Θ producing higher angular-momentum requirements) demonstrates the persistent role of both quantum-gravitational and electromagnetic effects in determining orbital characteristics.

Astrophysical Implications: Our results have important implications for understanding observational signatures of quantum gravitational effects in black hole systems. The systematic modifications of magnetic field configurations and ISCO parameters induced by the NC parameter Θ could be constrained by observations of accretion disk spectra, particularly the iron Kα line profiles, which are sensitive to the inner disk radius. The energy efficiency of accretion, which depends on the ISCO location and binding energy, would be systematically affected by NC corrections, potentially providing another observational constraint on Θ. Furthermore, the modified magnetic field structure could influence jet formation and collimation processes, affecting the observable properties of relativistic jets from active galactic nuclei and microquasars.

Comparison with Modified Gravity Theories: The effects of non-commutative geometry on particle dynamics and electromagnetic fields can be compared with those arising from other modified gravity theories, such as Einstein-Maxwell-scalar theory, modified gravity (MOG), and Rastall gravity. While these theories produce qualitatively similar modifications to the ISCO radius and energy efficiency, the specific functional dependence on the respective parameters differs, potentially allowing observational discrimination. The unique feature of NC black holes is the regularization of spacetime singularities, combined with modifications to strong-field dynamics, which together offer a physically motivated framework rooted in quantum gravity considerations.

Future Directions: Several promising avenues for future research emerge from this work. First, extending the analysis to rotating (Kerr-like) NC black holes would enable investigation of frame-dragging effects on magnetic field configurations and particle dynamics in quantum-corrected spacetimes. Second, incorporating more realistic magnetic field geometries, such as those arising from magnetohydrodynamic simulations of accretion flows, would provide a more complete picture of black hole magnetospheres in NC geometry. Third, investigating radiation processes such as synchrotron emission and bremsstrahlung from charged particles in NC black hole magnetospheres could yield direct observational predictions testable with current and future X-ray observatories. Finally, exploring the role of NC corrections in extreme particle-acceleration scenarios, such as the Penrose process and magnetically driven acceleration mechanisms, could shed light on the origin of ultra-high-energy cosmic rays.

In conclusion, our investigation demonstrates that noncommutative geometry induces measurable, systematic modifications to electromagnetic field structures and to the dynamics of charged particles around black holes. These findings contribute to the broader effort to understand quantum-gravitational effects in strong-field regimes and provide testable signatures that could be constrained or detected through multi-messenger astronomical observations of black hole systems. The interplay between quantum gravity corrections and electromagnetic phenomena is a rich area for future theoretical and observational research, with implications that extend from fundamental physics to high-energy astrophysics.

REFERENCES

[1] S. W. Hawking and G. F. R. Ellis. The Large Scale Structure of Space-Time. *Cambridge Monographs on Mathematical Physics*, 1973.

[2] Piero Nicolini, Anais Smailagic, and Euro Spallucci. Noncommutative geometry inspired Schwarzschild black hole. *Physics Letters B*, 632(4):547–551, January 2006.

[3] Piero Nicolini, Anais Smailagic, and Euro Spallucci. The Fate of radiating black holes in noncommutative geometry. 7 2005.

[4] Stefano Ansoldi, Piero Nicolini, Anais Smailagic, and Euro Spallucci. Noncommutative geometry inspired charged black holes. *Phys. Lett. B*, 645:261–266, 2007.

[5] Euro Spallucci, Anais Smailagic, and Piero Nicolini. Non-commutative geometry inspired higher-dimensional charged black holes. *Phys. Lett. B*, 670:449–454, 2009.

[6] Nathan Seiberg and Edward Witten. String theory and noncommutative geometry. *JHEP*, 09:032, 1999.

[7] Sergio Doplicher, Klaus Fredenhagen, and John E. Roberts. The Quantum structure of space-time at the Planck scale and quantum fields. *Commun. Math. Phys.*, 172:187–220, 1995.

[8] Piero Nicolini and Euro Spallucci. Noncommutative geometry inspired wormholes and dirty black holes. *Class. Quant. Grav.*, 27:015010, 2010.

[9] Piero Nicolini. Noncommutative Black Holes, The Final Appeal To Quantum Gravity: A Review. *Int. J. Mod. Phys. A*, 24:1229–1308, 2009.

[10] Javlon Rayimbaev, A. H. Bokhari, and Bobomurat Ahmedov. Quasiperiodic oscillations from noncommutative inspired black holes. *Class. Quant. Grav.*, 39(7):075021, 2022.

[11] Chikun Ding, Sheng Kang, Chiung-Yuan Chen, Shaowen Deng, and Chang Liu. Strong gravitational lensing in a noncommutative black-hole spacetime. *Phys. Rev. D*, 83:084005, 2011.

[12] R. D. Blandford and R. L. Znajek. Electromagnetic extraction of energy from Kerr black holes. *Mon. Not. Roy. Astron. Soc.*, 179:433–456, 1977.

[13] Robert M. Wald. Black hole in a uniform magnetic field. *Phys. Rev. D*, 10:1680–1685, 1974.

[14] Jacobus A. Petterson. Magnetic field of a current loop around a Schwarzschild black hole. *Phys. Rev. D*, 10:3166–3170, 1974.

[15] A. A. Abdujabbarov, B. J. Ahmedov, and V. G. Kagramanova. Particle Motion and Electromagnetic Fields of Rotating Compact Gravitating Objects with Gravitomagnetic Charge. *Gen. Rel. Grav.*, 40:2515–2532, 2008.

[16] A. A. Abdujabbarov, B. J. Ahmedov, and N. B. Jurayeva. Charged-particle motion around a rotating non-Kerr black hole immersed in a uniform magnetic field. *Phys. Rev. D*, 87:064042, 2013.

[17] V. P. Frolov and A. A. Shoom. Motion of charged particles near a weakly magnetized Schwarzschild black hole. *Phys. Rev. D*, 82:084034, 2010.

[18] Javlon Rayimbaev, Ahmadjon Abdujabbarov, and Cosimo Bambi. Magnetized particle motion around non-Schwarzschild black hole immersed in an external uniform magnetic field. *Phys. Rev. D*, 102(8):084016, 2020.

[19] B. Narzilloev, J. Rayimbaev, A. Abdujabbarov, and C. Bambi. Charged particle motion around non-singular black holes in conformal gravity in the presence of external magnetic field. *Eur. Phys. J. C*, 80(11):1074, 2020.

[20] J. Vrba, A. Abdujabbarov, M. Kološ, B. Ahmedov, Z. Stuchlík, and J. Rayimbaev. Charged particle motion in Reissner-Nordström spacetimes with non-zero cosmological constant. *Phys. Rev. D*, 101(12):124039, 2020.

[21] I. D. Novikov and K. S. Thorne. Astrophysics of black holes. *Black Holes (Les Astres Occlus)*, pages 343–450, 1973.

[22] Don N. Page and Kip S. Thorne. Disk-Accretion onto a Black Hole. Time-Averaged Structure of Accretion Disk. *Astrophys. J.*, 191:499–506, 1974.

[23] Leonardo Modesto. Disappearance of black hole singularity in quantum gravity. *Phys. Rev. D*, 70:124009, 2004.

[24] Rabin Banerjee, Bibhas Ranjan Majhi, and Sujoy Samanta. Noncommutative Black Hole Thermodynamics. *Phys. Rev. D*, 77:124035, 2008.

[25] Zdeněk Stuchlík and Martin Kološ. Acceleration of the charged particles due to chaotic scattering in the combined black hole gravitational field and asymptotically uniform magnetic field. *Eur. Phys. J. C*, 76(1):32, 2016.

[26] Martin Kološ, Arman Tursunov, and Zdeněk Stuchlík. Possible signature of magnetic fields related to quasi-periodic oscillations observed in microquasars. *Eur. Phys. J. C*, 77(12):860, 2017.

[27] R. M. Wald. Black hole in a uniform magnetic field. *Phys. Rev. D*, 10:1680–1685, September 1974.

[28] Ahmadjon Abdujabbarov, Javlon Rayimbaev, Bobur Turimov, and Farruh Atamurotov. Dynamics of magnetized particles around 4-D Einstein Gauss-Bonnet black hole. *Physics of the Dark Universe*, 30:100715, December 2020.

[29] Muhammad Zahid, Javlon Rayimbaev, Saeed Ullah Khan, Jingli Ren, Saidmuhammad Ahmedov, and Inomjon Ibragimov. Dynamics and collisions of magnetized particles around charged black holes in Einstein–Maxwell-scalar theory. *Eur. Phys. J. C*, 82(5):494, 2022.

[30] Jaroslav Vrba, Ahmadjon Abdujabbarov, Martin Kološ, Bobomurat Ahmedov, Zdeněk Stuchlík, and Javlon Rayimbaev. Charged and magnetized particles motion in the field of generic singular black holes governed by general relativity coupled to nonlinear electrodynamics. *Phys. Rev. D*, 101(12):124039, 2020.

